Transcriptase XL. Polymerase chain reaction (PCR) was performed in a 100 μl reaction solution containing 5 units TaKaRa LA Taq for 40 cycles using synthetic primers, which were designed using conserved regions in the coding sequence of the previously identified Tg sequences of four mammalian species, bovine, human, murine and rat, such that nine overlapping regions of approximately 1–2 kb in length were amplified (Table 1). The amplification of cDNA was performed for 40 cycles of 30 s at 94 °C, 30 s at the specific annealing temperature, and 2 min at 72 °C. The first cycle was preceded by a denaturation of 2 min at 94 °C and the last cycle was followed by a final extension of 5 min at 72 °C.

2.2. *Circular first-strand cDNA-mediated RACE method of the 5′ end of cTg mRNA*

The 5′ end of cTg mRNA was identified by the modified cRACE method using 5′-Full RACE core set (TaKaRa, Shiga, Kyoto). cDNA synthesis was performed as described above, with a phosphorylated downstream gene-specific primer (LA-PCR3, Table 1), located approximately 600 nucleotides from the putative transcription start. After hydrolysis of the template mRNA at 37 °C for 1 h, the cDNA was precipitated with ethanol and redissolved in 40 μl of RNA Ligation buffer containing 20% polyethylene glycol. After 40 units T4 RNA ligase was added, this ligation mixture was incubated at 15 °C for 16 h and an aliquot was directly used as a template for the amplification with gene-specific primers (LA-PCR4 and LA-PCR5, Table 1). The reaction was carried out for 40 cycles of 30 s denaturation at 94 °C, 30 s annealing at 58 °C and 1 min extension at 72 °C. The first cycle was preceded by a denaturation of 2 min at 94 °C and the last cycle was followed by a final extension of 5 min at 72 °C.

2.3. *Cloning and sequencing*

The PCR products were cloned into pT7Blue-2 plasmid vector (Novagen, Madison, WI) and pGEM®-T Easy vector (Promega, Madison, WI), according to the manufacture's recommendations. The sequence of the plasmid inserts was determined by automated DNA

Table 1
Sequence (5′ → 3′) of the primers used for PCR cloning of canine thyroglobulin

Clones	T_{ann} (°C)	Upstream primer	Downstream primers
A	56	CTCACTAGGTGGTGAGGA	GTTTTCCCAGTCACGAC + T tail
B	58	GAGTTCCATATGCTGCCCC	GGATTTCCTGATCTGATGAAG
C	60	GCAAACCTGTGGTGCCTTTC	GCAGCTGGCCCTTGGCTT
D	62	TACCGAGCCAGCCAGAAGGAC	TCTATCTTCCAGCACAACTTTC
E	55	GAGTGATCGTGTGTGAGC	CCATAGAAATCACAGGAGAC
F	52	GAAGATCATGAGCTACAGA	CGGGAGCAGGAGCTG
G	56	CTTCAGTCAGTTTTTTCCAGC	GAGCGCTGAAGTCTGAGTA
H	56	GCAGCTACATTAACAGCA	CATCCTCGTAGTCTCCTTC
LA-PCR			CATACACCTCCATCCCTTC (LA3)
	56	GAGCGGCTACCTTAACA (LA5)	CTGCAGCTGACAGAATGACA (LA4)

Note: T_{ann} is the annealing temperature used in PCR.

sequencing using a BigDye® Terminator v1.1 Cycle Sequencing kit and a 3700 DNA sequence analyzer (Applied Biosystems, Foster City, CA).

2.4. Sequencing analysis

The determined DNA sequences data were analyzed using the program of GENETYX-Mac (Software Development, Sibuya, Tokyo) for sequence editing and analysis. The search for functional motifs of the predicted polypeptides was performed at the Sequence Motif Search website (http://motif.genome.jp).

3. Results

The nucleotide sequence of cTg mRNA was deduced by RT-PCR, cloning, and subsequent sequencing of nine overlapping plasmid cDNA clones. The nucleotide sequence revealed an open reading frame of 8289 nucleotides, preceded by a 41-nucleotide 5′ end-untranstated region, and followed by a 128-nucleotide 3′ end-untranslated region, containing the canonical polyadenylation signal (AAUAA). The cTg nucleotide sequence predicted a polypeptide of 2762 amino acids (Fig. 1). A leader peptide of 19 amino acids was followed by a 2743-amino-acid polypeptide, corresponding to the monomeric cTg. The amino acid composition indicated a rather high amount of leucine and serine residues (9.70 and 9.20%, respectively), and a small proportion of methionine (1.16%). Hydrophobic and charged amino-acid residues were homogeneously distributed on the polypeptide, whereas cysteine involved in the repetitive structures. The monomeric cTg polypeptide contained 66 tyrosine residues, representing 2.39% of total. The homology of cTg with the bovine, human, murine and rat Tg was 78.9, 78.1, 70.2, and 69.5%, respectively, at the amino acid level, and sequence databases searches confirmed that human acetylcholinesterase has the strongest mach, with 31% identity with the cTg sequence. Analysis of the deduced amino acid sequence revealed the existence of the repeated domain, thyroglobulin type-1. This domain was exclusively present in the N-terminal portion of the molecule, and was repeated nine times. It was composed of approximately 65 amino acids, in which the position of cysteine, proline, and glycine residues were highly conserved. The proportion of cysteine and tyrosine in the type-1 domain was high, as compared to the entire protomer. With type-1 domain, the amino acid sequence of cTg contained many functional motifs, 16 potential *N*-glycosylation sites, three cAMP- and cGMP-dependent protein kinase phosphorylation sites, 1 carboxylesterases type-B signature 2, 1 amidation site, 35 protein kinase C phosphorylation sites, 3 tyrosine kinase phosphorylation sites, 49 *N*-myristoylation sites, 50 casein kinase II phosphorylation sites and 1 leucine zipper pattern (Fig. 2).

4. Discussion

The analysis of the amino acid sequence of cTg, as deduced from its mRNA, revealed the polypeptide of 2762 amino acids. Homology analysis showed that cTg is closely related

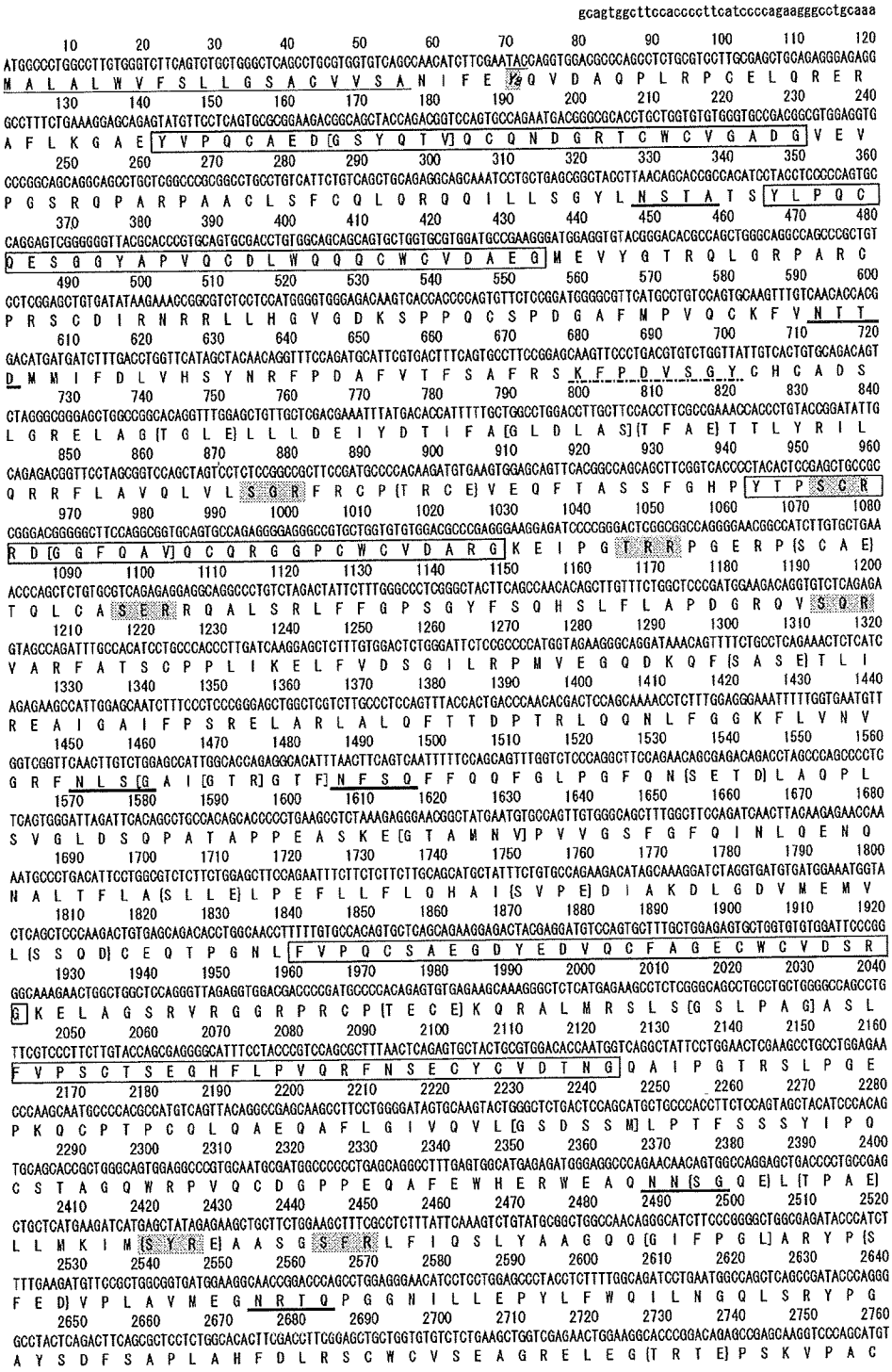

Fig. 1. Nucleotide sequence of canine thyroglobulin cDNA, and the deduced sequence of the protein. The last three sequences, TGA (*) is stop codon: XXX, leader peptide; XXX , cAMP- and cGMP-dependent protein kinase phosphorylation site; XXX , *N*-glycosylation site; XXX , carboxylesterase type-B signature 2; XXX , amidation site; XXX , protein kinase C phosphorylation site; XXX , tyrosine kinase phosphorylation site; [XXX] , *N*-myristoylation site; {XXX} , casein kinase II phosphorylation site; XXX , thyroglobulin type 1 repeat signature; Yx , tyrosine residues A–D.

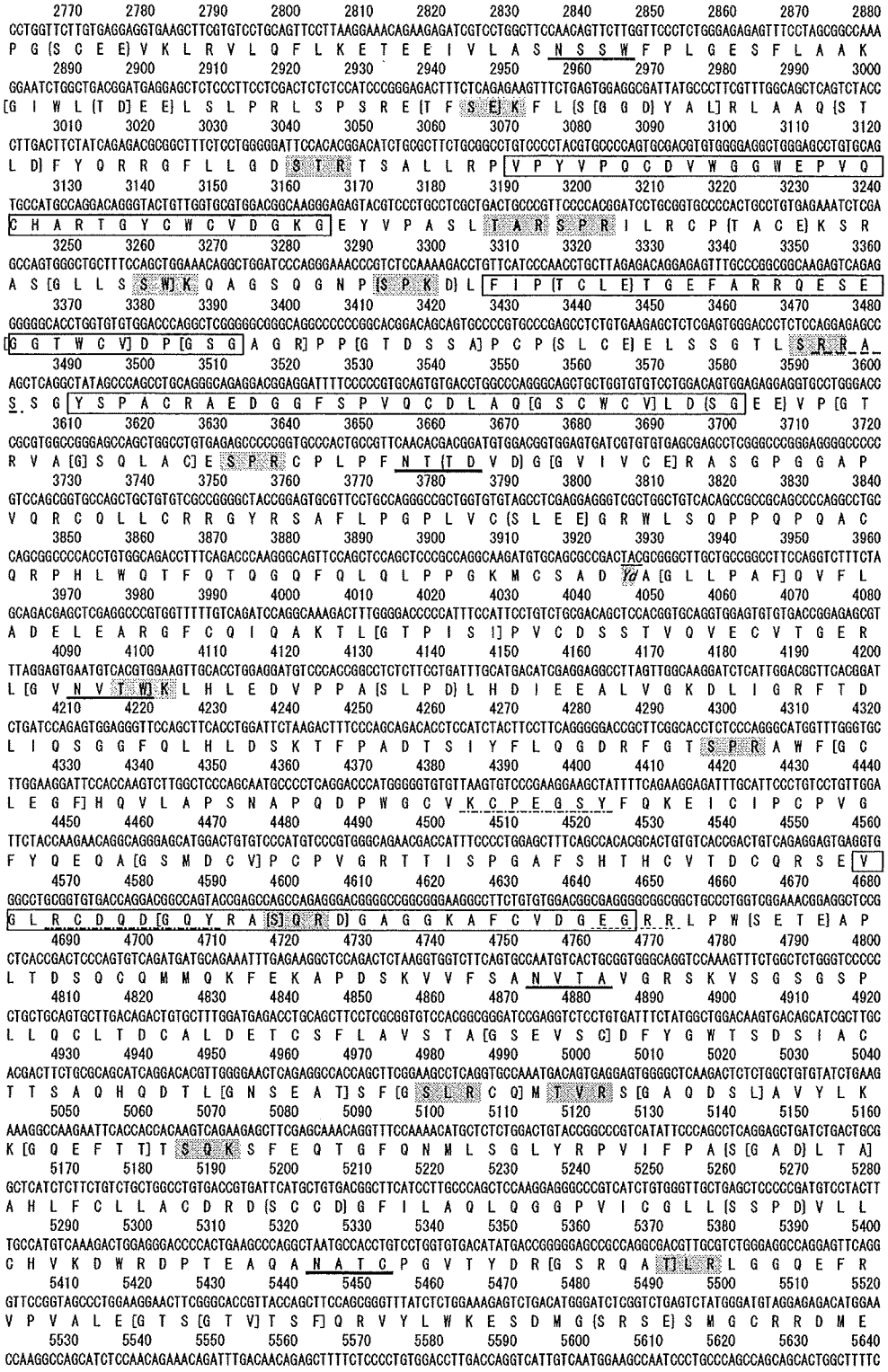

Fig. 1. (*Continued*)

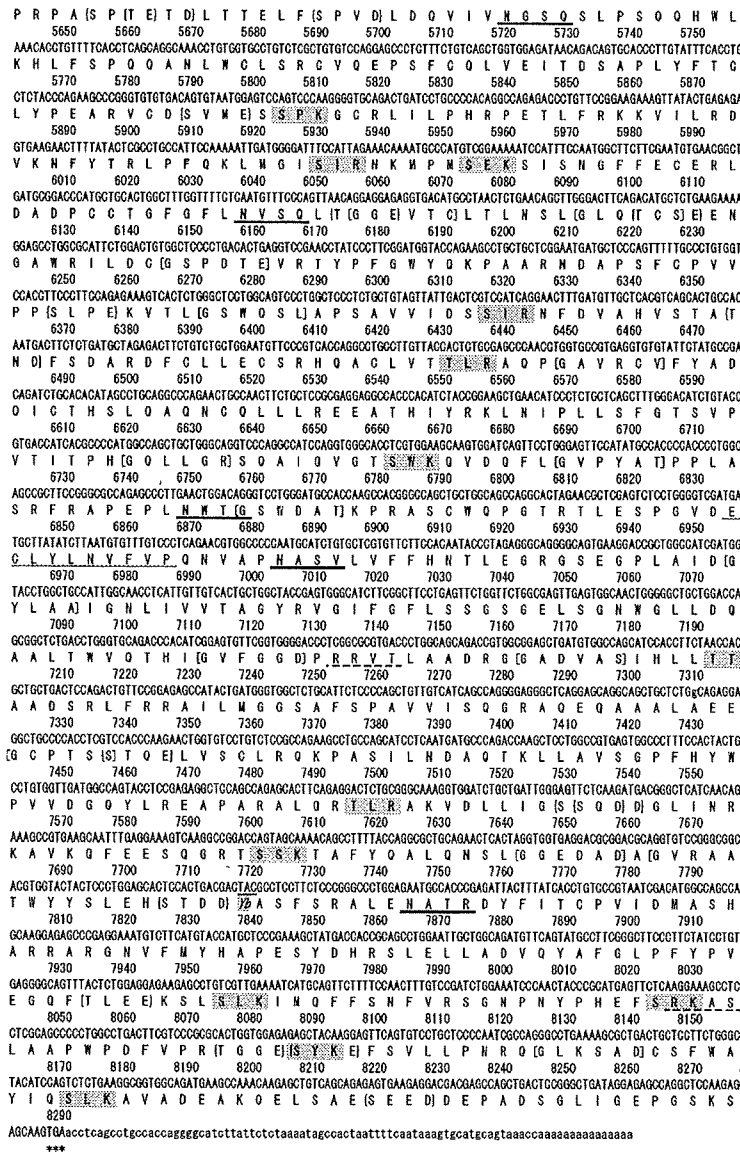

Fig. 1. (*Continued*).

to different species and especially 78.9 and 78.1% identical to bovine and human Tg, respectively. Similarly to bovine and human Tg, in cTg the most represented amino acids are serine and leucine, and the least represented are methionine and histidine [13,14]. The most conserved amino acid is cysteine, whose number and location is almost invariable among bovine, human, murine and rat Tg. The tyrosine residues, which are iodinated for the synthesis of thyroid hormones, are also well conserved in cTg. In the dog, 8 locations among 66 tyrosine residues are different between canine and human Tg. Among these eight substitutions, six tyrosine residues are replaced by aromatic amino acids, histidine and phenylalanine. Marriq et al. [17] and Rawitch et al. [18] demonstrated that four of the tyrosine residues are involved as 'acceptor' sites in thyroxine and triiodothyronine

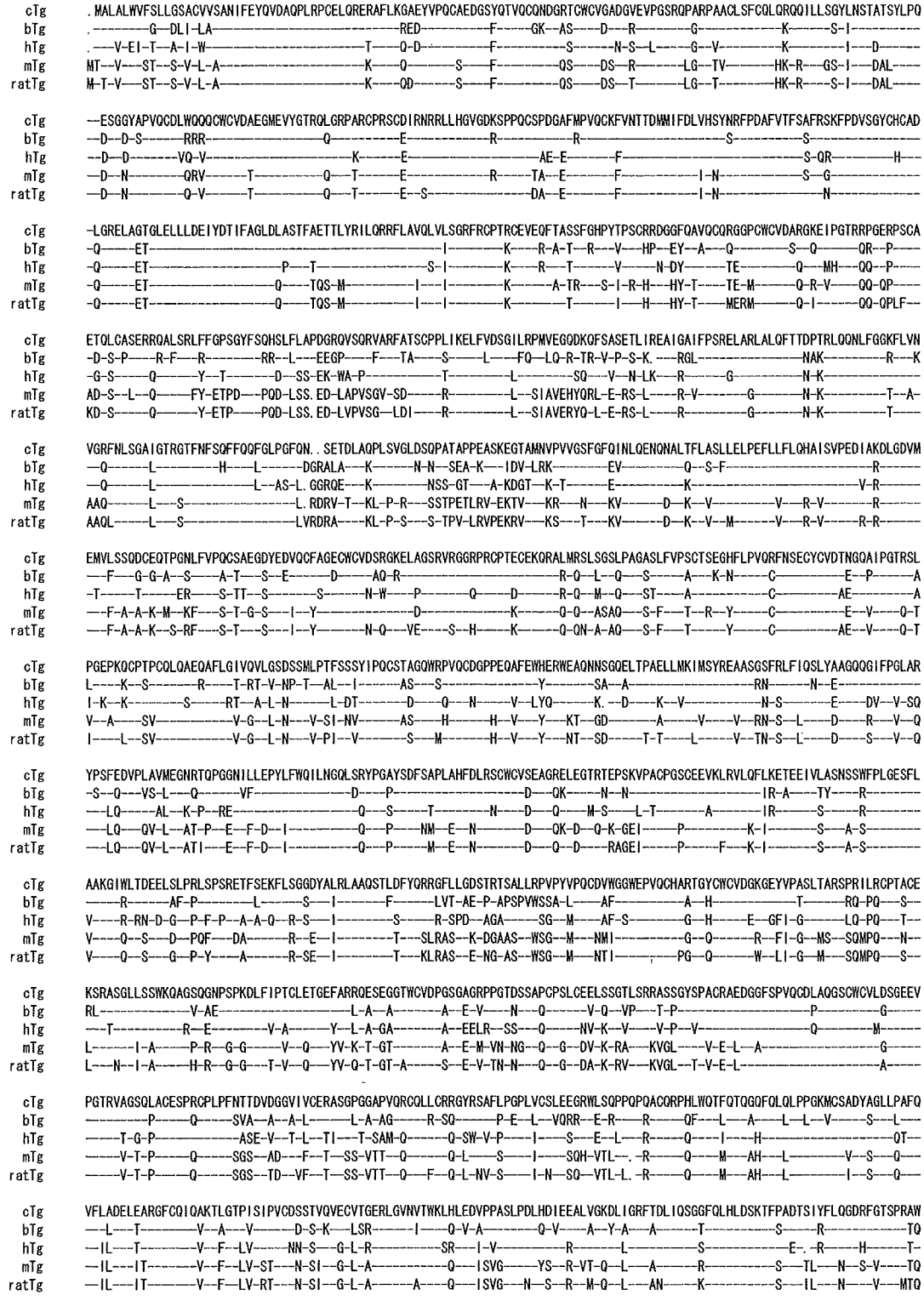

Fig. 2. Alignment of canine, bovine, human, murine, and rat thyroglobulin. The dash indicates the conserved amino acid compared with canine Tg, and dots indicate positions where the amino acid residues are missing.

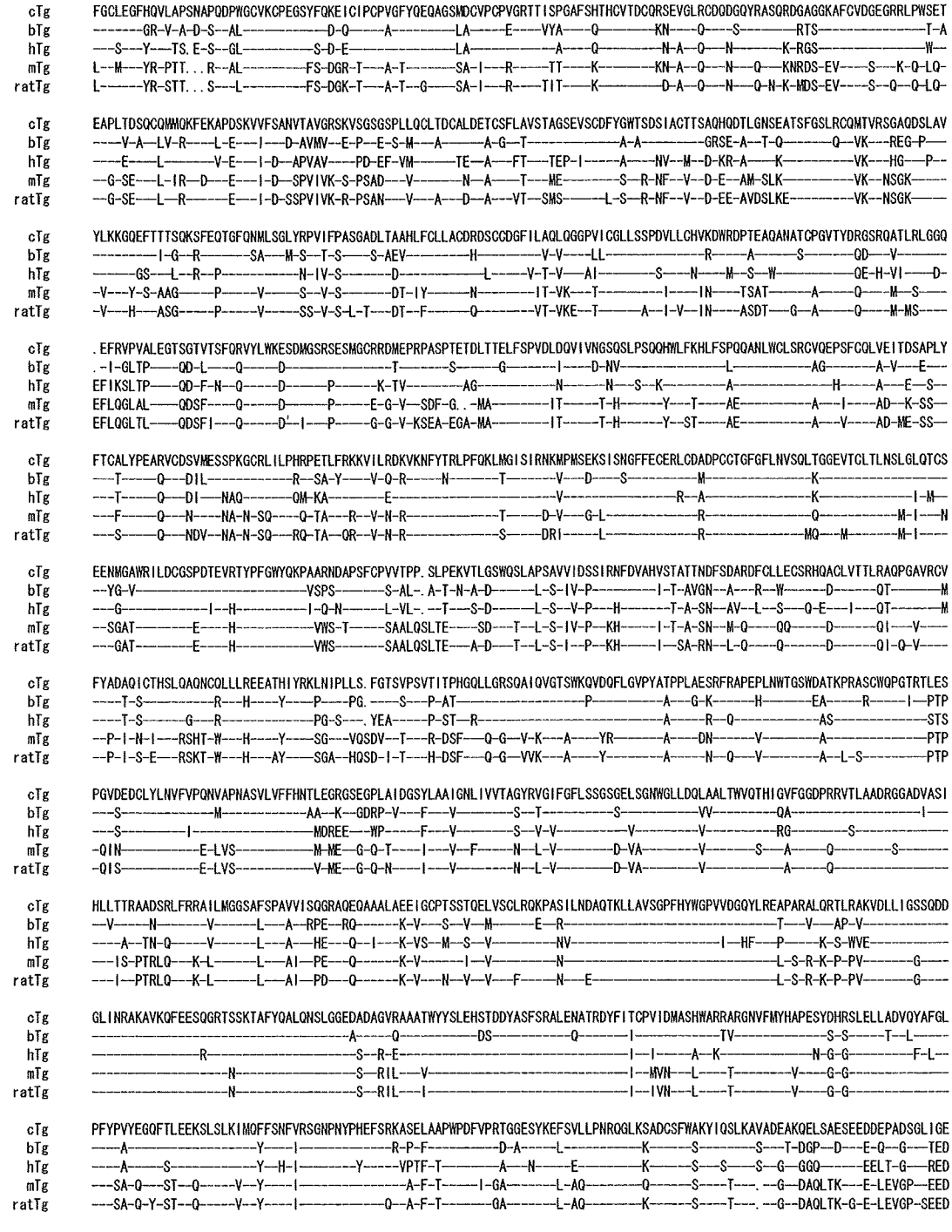

Fig. 2. (*Continued*).

formation. Under physiological conditions, only four tyrosines are available for iodination and hormonogenesis and these tyrosines are designated A–D [13,15,19]. These four major hormonogenic sites are highly conserved among the species. In the cTg sequence, these sites are also identified (Fig. 1). The hormonogenic site A is usually located within 30 amino acids, like as the first Tg-type 1 repeat [20,21]. Sites B–D are located at 2573, 2760 and 1309 amino acid, respectively. Analysis for internal homologies confirmed the presence of one domain, about 65 amino acids, repeated 11 times (Fig. 1). This domain, known as thyroglobulin type-1, also is described in the bovine and human Tg sequence and identified in other proteins of different origin and function [22]. It likely represents the duplication of ancestral genes [20,21], and can act as proteinase inhibitors in other proteins [22,23]. It is hypothesized that the type-1 repeats in Tg could act as pH-dependent blinders and reversible inhibitors of the proteases implicated in Tg degradation and T_4 release [24]. However, the definite function for this type of repeat in Tg has not been established yet. Sequence databases searches revealed the strongest match between cTg and acetylcholinesterase (31% identity). Acetylcholinesterase has the strongest match, with 31% identity with cTg. The native structure of the AChE-like region functions as a dimerization domain, facilitating intracellular transport of Tg to the site of thyroid hormonogenesis [25]. However, the putative function of AChE-like region in Tg is not clear, but as acetylcholinesterase interacts with cell membranes in the nervous system a similar role for the homologous domain at the carboxy-terminal end of the Tg molecule has been proposed for apical membrane interaction. In *cog/cog* mice, Tg secretion defect is associated with a single L2263P substitution that falls within the AChE homology domain [26]. Unfortunately, the mutation in *cog/cog* mice located in this domain leads to ER storage of apparently misfolded Tg molecules [26] and therefore does not directly contribute to the elucidation of the function of this domain. Patients with congenital goitrous hypothyroidism and defective Tg, as well as animal models of the human diseases, have been recognized for many years. The thyrocytes in such patients typically exhibit a dilated ER lumen [27] with little or no secreted Tg [28]. Mutations in a variety of Tg regions can result in goitrous hypothyroidism as a result of deficiency of Tg folding [16,29]. The homologous regions of cTg and acetylcholinesterase, AChE-like region, may be the target epitopes of autoimmune thyroid diseases [14,30].

In the pathogenic mechanism of autoimmune diseases, T- and B-cell epitopes have important roles. Several T-cell epitopes were reported in human and rat Tg peptides [31–34]. About B-cell epitopes, Saboori and others reported conformation-dependent epitopes [35–38]. Previously, we have identified tryptic peptides bearing non-conformational epitopes, suggesting that specific peptides, not conformational, were involved in the TgAA induction in dog as being compared with human Tg [39]. However, we have not yet analyzed these tryptic peptides, and have not enough information as to the localization of epitopes on cTg.

Presently, the predicted cDNA sequence of cTg was registered in the data bank from canine genome project (XM_539168). We compared it with our complete cDNA sequence. In the analysis results, although there was 99% homology between two sequences, we found several missing and varying amino acids sequences (data not shown). We could not determine whether these unmatched sequences were simple analytic errors or not. But, the present complete cDNA sequence was analyzed directly by RT-PCR method from mRNA. However, it is believed that these two sequences from different sources could provide available information about mutation, substitution or deletion on cTg.

In conclusion, we analyzed the complete primary structure of cTg, deducing it from the cDNA sequence, and to compare it with human and other Tg sequences to identify canine specific areas. Defects in the structure of cTg are considered linked to the existence of hereditary thyroid diseases in dog, and knowledge of the primary structure of cTg and the corresponding gene facilitates the development of studies on the structural bases of defects in Tg production. These results could be useful to further research about mutations of cTg, epitopes mapping associated with autoimmune thyroid diseases and structure–function relationship on cTg.

References

[1] Gosselin SJ, Capen CC, Martin SL. Histologic and ultrastructural evaluation of thyroid lesions associated with hypothyroidism in dogs. Vet Pathol 1981;18:299–309.
[2] Lee J-Y, Uzuka Y, Tanabe S, Sarashina T. Prevalence of thyroglobulin autoantibodies detected by enzyme-linked immunosorbent assay of canine serum in hypothyroid, obese and healthy dogs in Japan. Res Vet Sci 2004;76(2):129–32.
[3] Greenspan FS. The thyroid gland. In: Greenspan FS, Gardner DG, editors. Basic and clinical endocrinology. New York: Lange Medical Books/McGraw-Hill; 2003. p. 215–94.
[4] Panciera DL. Hypothyroidism in dogs: 66 cases. J Am Vet Med Assoc 1994;204:761–7.
[5] Thrasyvoulides A, Sakarellos-Daitsiotis M, Philippou G, Souvatzoglou A, Sakarellos C, Lymberi P. B-cell autoepitopes on the acetylcholinesterase-homologous region of human thyroglobulin: association with Graves' disease and thyroid eye disease. Eur J Endocrinol 2001;145(2):119–27.
[6] Beale KM, Halliwell RE, Chen CL. Prevalence of antithyroglobulin antibodies detected by enzyme-linked immunosorbent assay of canine serum. J Am Vet Med Assoc 1990;196:745–8.
[7] Beale KM. Thyroid pathology and serum antithyroid antibodies in hypothyroid and healthy dogs. J Vet Intern Med 1991;5:128.
[8] Feldman EC, Nelson RW. Canine hypothyroidism. In: Canine and feline endocrinology and reproduction. Philadelphia: WB Saunders Co.; 2004. p. 88–142.
[9] Brazillet MP, Batteux F, Abehsira-Amar O, Nicoletti F, Charreire J. Induction of experimental autoimmune thyroiditis by heat-denatured porcine thyroglobulin: a Tc1-mediated disease. Eur J Immunol 1999;29(4):1342–52.
[10] Brazillet MP, Mignon-Godefroy K, Charreire J. Induction of experimental autoimmune thyroiditis (EAT) by heat-denaturated thyroglobulin (Tg). Exp Clin Endocrinol Diabetes 1996;104(3):23–5.
[11] Van Ommen GJ, Sterk A, Mercken LO, Arnberg AC, Baas F, De Vijlder JJ. Studies on the structures of the normal and abnormal goat thyroglobulin genes. Biochimie 1989;71(2):211–21.
[12] Lee J-Y, Uzuka Y, Tanabe S, Takasawa T, Sarashina T, Nachreiner RF. Tryptic peptides of canine thyroglobulin reactive with sera of patients with canine hypothyroidism caused by autoimmune thyroiditis. Vet Immunol Immunopathol 2004;101(3–4):271–6.
[13] Mercken L, Simons MJ, Swillens S, Massaer M, Vassart G. Primary structure of bovine thyroglobulin deduced from the sequence of its 8, 431-base complementary DNA. Nature 1985;316(6029):647–51.
[14] Malthiery Y, Lissitzky S. Primary structure of human thyroglobulin deduced from the sequence of its 8448-base complementary DNA. Eur J Biochem 1987;165(3):491–8.
[15] Caturegli P, Vidalain PO, Vali M, Aguilera-Galaviz LA, Rose NR. Cloning and characterization of murine thyroglobulin cDNA. Clin Immunol Immunopathol 1997;85(2):221–6.
[16] Hishinuma A, Furudate S, Oh-Ishi M, Nagakubo N, Namatame T, Ieiri T. A novel missense mutation (G2320R) in thyroglobulin causes hypothyroidism in rdw rats. Endocrinology 2000;141(11):4050–5.
[17] Marriq C, Rolland M, Lissitzky S. Structure–function relationship in thyroglobulin: amino acid sequence of two different thyroxine-containing peptides from porcine thyroglobulin. EMBO J 1982;1(4):397–401.
[18] Rawitch AB, Chernoff SB, Litwer MR, Rouse JB, Hamilton JW. Thyroglobulin structure–function. The amino acid sequence surrounding thyroxine. J Biol Chem 1983;258(4):2079–82.

[19] Dunn JT, Anderson PC, Fox JW, Fassler CA, Dunn AD, Hite LA, et al. The sites of thyroid hormone formation in rabbit thyroglobulin. J Biol Chem 1987;262(35):16948–52.
[20] Ludgate M, Swillens S, Mercken L, Vassart G. Homology between thyroglobulin and acetylcholinesterase: an explanation for pathogenesis of Graves' ophthalmopathy? Lancet 1986;2(8500):219–20.
[21] Matsiota P, Blancher A, Doyon B, Guilbert B, Clanet M, Kouvelas ED, et al. Comparative study of natural autoantibodies in the serum and cerebrospinal fluid of normal individuals and patients with multiple sclerosis and other neurological diseases. Ann Inst Pasteur Immunol 1988;139(1):99–108.
[22] Wood AW, Matsumoto J, Van Der Kraak G. Thyroglobulin type-1 domain protease inhibitors exhibit specific expression in the cortical ooplasm of vitellogenic rainbow trout oocytes. Mol Reprod Dev 2004;69(2):205–14.
[23] Lenarcic B, Bevec T. Thyropins—new structurally related proteinase inhibitors. Biol Chem Feb 1998;379(2):105–11.
[24] Molina F, Pau B, Granier C. The type-1 repeats of thyroglobulin regulate thyroglobulin degradation and T3, T4 release in thyrocytes. FEBS Lett 1996;391(3):229–31.
[25] Park Y-N, Arvan P. The acetylcholinesterase homology region is essential for normal conformational maturation and secretion of thyroglobulin. J Biol Chem 2004;279(17):17085–9.
[26] Kim PS, Hossain SA, Park YN, Lee I, Yoo SE, Arvan P. A single amino acid change in the acetylcholinesterase-like domain of thyroglobulin causes congenital goiter with hypothyroidism in the cog/cog mouse: a model of human endoplasmic reticulum storage diseases. Proc Natl Acad Sci USA 1998;95(17):9909–13.
[27] Medeiros-Neto G, Targovnik H, Knobel M, Propato F, Varela V, Alkmin M, et al. Qualitative and quantitative defects of thyroglobulin resulting in congenital goiter. Absence of gross gene deletion of coding sequences in the TG gene structure. J Endocrinol Invest 1989;12(11):805–13.
[28] Medeiros-Neto G, Kim PS, Yoo SE, Vono J, Targovnik HM, Camargo R, et al. Congenital hypothyroid goiter with deficient thyroglobulin. Identification of an endoplasmic reticulum storage disease with induction of molecular chaperones. J Clin Invest 1996;98(12):2838–44.
[29] Van de Graaf SA, Ris-Stalpers C, Pauws E, Mendive FM, Targovnik HM, de Vijlder JJ. Up to date with human thyroglobulin. J Endocrinol 2001;170(2):307–21.
[30] Schumacher M, Camp S, Maulet Y, Newton M, MacPhee-Quigley K, Taylor SS, et al. Primary structure of Torpedo californica acetylcholinesterase deduced from its cDNA sequence. Nature 1986;319(6052):407–9.
[31] Champion BR, Rayner DC, Byfield PG, Page KR, Chan CT, Roitt IM. Critical role of iodination for T cell recognition of thyroglobulin in experimental murine thyroid autoimmunity. J Immunol 1987;139(11):3665–70.
[32] Champion BR, Page KR, Parish N, Rayner DC, Dawe K, Biswas-Hughes G, et al. Identification of a thyroxine-containing self-epitope of thyroglobulin which triggers thyroid autoreactive T cells. J Exp Med 1991;174(2):363–70.
[33] Texier B, Bedin C, Tang H, Camoin L, Laurent-Winter C, Charreire J. Characterization and sequencing of a 40-amino-acid peptide from human thyroglobulin inducing experimental autoimmune thyroiditis. J Immunol 1992;148(11):3405–11.
[34] Carayanniotis G, Rao VP. Searching for pathogenic epitopes in thyroglobulin: parameters and caveats. Immunol Today 1997;18(2):83–8.
[35] Saboori AM, Burek CL, Rose NR, Bresler HS, Talor M, Kuppers RC. Tryptic peptides of human thyroglobulin. I. Immunoreactivity with murine monoclonal antibodies. Clin Exp Immunol 1994;98(3):454–8.
[36] Saboori AM, Caturegli P, Rose NR, Mariotti S, Pinchera A, Burek CL. Tryptic peptides of human thyroglobulin. II. Immunoreactivity with sera from patients with thyroid diseases. Clin Exp Immunol 1994;98(3):459–63.
[37] Saboori AM, Rose NR, Burek CL. Amino acid sequence of a tryptic peptide of human thyroglobulin reactive with sera of patients with thyroid diseases. Autoimmunity 1995;22(2):87–94.
[38] Saboori AM, Rose NR, Yuhasz SC, Amzel LM, Burek CL. Peptides of human thyroglobulin reactive with sera of patients with autoimmune thyroid disease. J Immunol 1999;163(11):6244–50.
[39] Lee JY, Uzuka Y, Tanabe S, Takasawa T, Sarashina T, Nachreiner RF. Tryptic peptides of canine thyroglobulin reactive with sera of patients with canine hypothyroidism caused by autoimmune thyroiditis. Vet Immunol Immunopathol 2004;101(3–4):271–6.

Journal of Reproduction and Development, Vol. 53, No. 4, 2007

—Research Note—

Expression of Uterine Sensitization-Associated Gene-1 (USAG-1) in the Mouse Uterus During the Peri-Implantation Period

Kanami MAEDA[1)], Dong-Soo LEE[1)], Yoshiko YANAGIMOTO UETA[1)] and Hiroshi SUZUKI[1,2)]

[1)]Research Unit for Functional Genomics, National Research Center for Protozoan Diseases, Obihiro University of Agriculture and Veterinary Medicine, Nishi 2–13, Inada-cho, Obihiro, Hokkaido 080-8555 and [2)]Department of Developmental and Medical Technology, Graduate School of Medicine, The University of Tokyo, 7–3–1 Hongo, Bunkyo-ku, Tokyo 113-033, Japan

Abstract. Rat uterine sensitization-associated gene-1 (USAG-1) mRNA is expressed in the uterus during the peri-implantation period, and its mRNA expression in uterine epithelial cells is highest on day 5 of pregnancy. On the other hand, since changes in USAG-1 mRNA expression in the mouse uterus are not seen during the estrous cycle, USAG-1 expression might be specifically regulated by embryonic factors rather than by the maternal environment. However, the expression pattern and function of USAG-1 in the mouse uterus have not been determined. Thus, we examined the tissue-specific USAG-1 mRNA expression in the uteri of ICR mice during peri-implantation using real-time quantitative PCR. Uterine tissues, such as the myometrium, luminal epithelium, and stroma, were collected by laser capture microdissection at 3.5–6.5 dpc. USAG-1 mRNA was expressed in the uteri of pregnant mice from 3.5 dpc to 6.5 dpc, and the highest level of expression was seen at 4.5 dpc ($P<0.01$). Significantly high USAG-1 mRNA expression was detected in the luminal epithelium at 4.5 dpc ($P<0.05$). The stroma and myometrium exhibited unchanged expression levels of USAG-1 mRNA at 3.5–5.5 dpc. USAG-1 mRNA was undetectable in blastocysts and implanting embryos. Expression of USAG-1 mRNA appears to be associated with blastocyst implantation to the luminal epithelium, suggesting that physiological or biochemical contact of the blastocyst to the uterus is required for USAG-1 expression.

Key words: Implantation, Mouse, mRNA, Uterine sensitization-associated gene-1 (USAG-1), Uterus

(J. Reprod. Dev. 53: 931–936, 2007)

For successful establishment of pregnancy, blastocyst development must proceed beyond the attachment stage and result in endometrial decidualization and subsequent placental formation. Estrogen and progesterone regulate the events that lead to the receptivity and sensitization of the endometrium for the decidual cell reaction [1]. In rodents and humans, implantation is initiated with an apposition between the trophoblast and apical surface of the luminal epithelium. This is followed rapidly by adhesion of the conceptus to the luminal surface and then penetration through the luminal epithelium to the underlying stroma, which initiates the endometrial decidualization reaction [2, 3]. Uterine sensitization-associated gene-1 (USAG-1), a gene of unknown function during conceptus development, is upregulated in the sensitized endometrium of the rat uterus during the peri-implantation period [4].

Accepted for publication: February 13, 2007
Published online: March 28, 2007
Correspondence: H. Suzuki (e-mail: hisuzuki@obihiro.ac.jp)

This molecule is expressed as an antagonist to bone morphogenetic protein (BMP) in teeth [5] and the kidney renal tubules [6] during late embryogenesis. The homology of rat USAG-1 cDNA to those of mouse and human is 96% and 91%, respectively [7]. We previously identified USAG-1 mRNA expression in mouse uteri during the estrous cycle [8]. In contrast to the temporally regulated expressions of COX-1, COX-2, EGF, LIF, and other growth factors/cytokines, USAG-1 mRNA expression did not change during the estrous cycle [8]. However, the expression pattern and function of USAG-1 in the mouse uterus during the peri-implantation period have not been studied. Thus, we examined tissue-specific expression of USAG-1 mRNA in pregnant uteri and blastocyst stage embryos following dissection of various uterine tissues through laser microdissection.

Materials and Methods

Animals

ICR and (C57BL/6J × C3H/HeN)F1 mice at 8–10 weeks of age were purchased from a commercial supplier (CLEA Japan, Tokyo, Japan) and maintained in the animal facility of the National Research Center for Protozoan Diseases at Obihiro University of Agriculture and Veterinary Medicine, Obihiro, Japan. All animals were housed in polycarbonate cages and maintained in a specific pathogen-free environment in light-controlled (lights on from 07:00 to 19:00) and air-conditioned rooms (temperature of 24 ± 1 C, humidity of 50 ± 10%). They had access to standard laboratory chow (CE-2; CLEA Japan) and water *ad libitum*. The animals used in this study were cared for and used under the Guiding Principles for the Care and Use of Research Animals set forth by the Obihiro University of Agriculture and Veterinary Medicine.

Natural mating and tissue and embryo collection

Female mice were mated with fertile ICR males or vasectomized B6C3F1 males. The morning a vaginal plug was discovered was designated 0.5 days post coitum (dpc). Plug-positive females were sacrificed by cervical dislocation at 3.5–6.5 dpc. Five animals were sacrificed each day. The uteri of the animals were excised immediately immersed into liquid nitrogen, and stored at –80 C until use. For total RNA extraction from blastocysts, 200 blastocysts were collected from the uteri of naturally mated females at 3.5 dpc, immediately immersed in liquid nitrogen, and stored at –80 C until use.

Laser capture microdissection (LCM) of uterine tissues

Frozen uterine tissue from pregnant and pseudopregnant animals were embedded in OCT

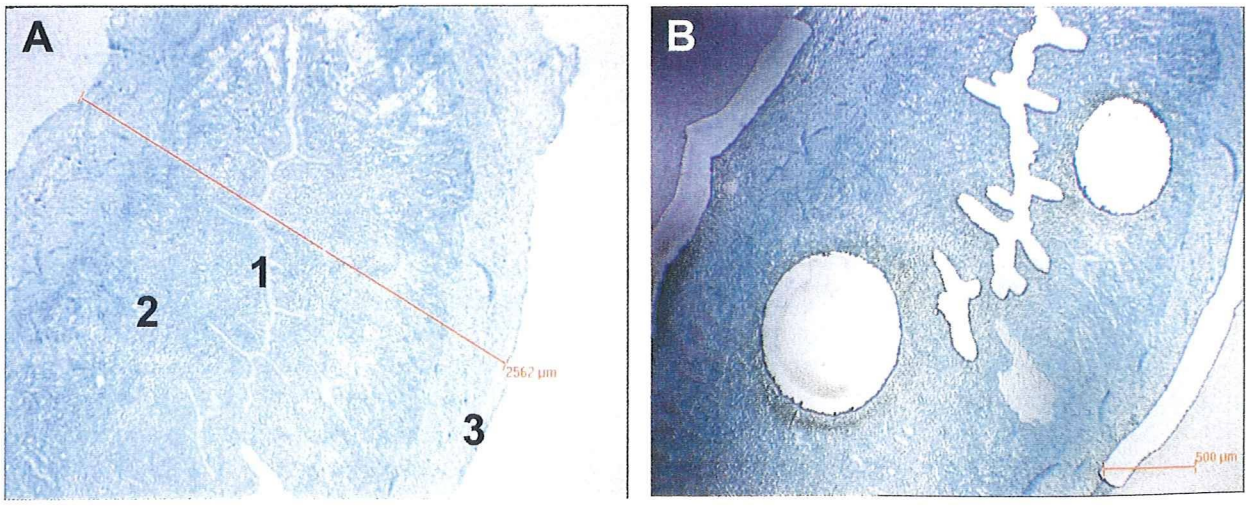

Fig. 1. Laser capture microdissection (LCM) of uterine tissues. LCM was performed using an AS LMD laser microdissection system (Leica) to separately collect attached blastocyst, myometrium, luminal epithelium and stromal tissue. The collected tissues were subjected to real-time quantitative PCR for detection of USAG-1 mRNA expression. A: before LCM. B: after LCM. 1. Luminal epithelium. 2. Stroma. 3. Muscle.

Table 1. Primer/probe sequence used for real-time quantitative PCR

Transcript	Primer/probe sequence (5′ to 3′)	GenBank accession number
USAG-1	F GAGGCAGGCATTTCAGTAGCA	NM_025312
	R TGTATTTGGTGGACCGCAGTT	
	FAM-TCGAAACAGTCGAGTTCA-MGB	
Beta-Actin	F GCTCTGGCTCCTAGCACCAT	NM_007393
	R GCCACCGATCCACACAGAGT	
	FAM-ATCAAGATCATTGCTCCTC-MGB	
18S rRNA	VIC-ABI (Part No. 4308329)	
	F ABI (Cat No. 430448604022)	
	R ABI (Cat No. 430449004024)	
GAPDH	VIC-ABI (Part No. 4308313)	
	F ABI (Cat No. 0412021)	
	R ABI (Cat No. 430410906026)	

compound (Tissue-Tech, Sakura, Tokyo, Japan). Serial cryostat sections were cut to 12–16 μm in thickness and mounted on autoclaved polyethylene naphthalate (PEN) foil on a glass slide (Leica, Wetzlar, Germany). The slides were fixed in 70% ethanol : acetic acid (19:1) for 3 min and briefly rinsed with RNase-free DEPC-treated water for 1 min. They were then stained with 0.05% toluidine blue (Merk, Darmstadt, Germany) dissolved in RNase-free DEPC-treated water for 1 min at room temperature and washed twice with RNase-free DEPC-treated water for 1 min each. The slides were then air-dried for 5 min and stored at –80 C.

LCM was performed using an AS LMD laser microdissection system (Leica) to collect the attached blastocyst, myometrium, luminal epithelium, and stromal tissues separately [9]. PEN foil slides were mounted on an AS LMD laser microdissection system with the section facing downwards. After adjusting the intensity, aperture, and cutting velocity, the pulsed UV laser beam was carefully directed along the borders of the cell layer (Fig. 1). A 20x objective was used for the laser microdissection system along with the following settings: intensity was set to 45, aperture was set to 10, speed was set to 6, and offset was set to 39. The separated tissues were transferred by gravity alone into a microcentrifuge tube cap containing TRI reagent (Sigma, St. Louis, MO, USA) that was placed directly underneath the sections.

Real-time quantitative PCR

Total RNA was extracted from frozen reproductive tissues and blastocysts by means of a TRI Reagent Kit (Sigma) according to the manufacturer's protocol. The extracted total RNA was then subjected to real-time PCR analysis. Primers and a TaqMan probe for the USAG-1 gene and beta-actin [8] were designed using the primer design software Primer Express version 1.5 (Applied Biosystems, Foster City, CA, USA). Primers and a TaqMan probe for 18S rRNA and GAPDH were purchased from a commercial supplier (Applied Biosytems). The GenBank Accession numbers of all the cDNA sequences are summarized in Table 1. Quantification of all gene transcripts was carried out with an ABI Prism 7900 HT (Applied Biosystems). Templates for real-time PCR were obtained by reverse transcriptase reaction using total RNA. For the RT-PCR reaction, a TaqMan One-Step RT-PCR Master Mix Reagents Kit (Applied Biosystems) was used with 20 μl/tube as follows: the template (20 ng) was mixed with 2 × Master Mix without UNG, 40 × MultiScribe and RNAse Inhibitor Mix, 200 nM TaqMan Probe, and 900 nM of each primer. The reaction conditions were 1 cycle at 48 C for 30 min, 1 cycle at 95 C for 10 min, and then 45 cycles of the amplification step (95 C for 15 seconds and 60 C for 1 min). The gene expression levels of USAG-1 were calculated as gene expression rates, as reported previously [10]. Briefly, the amounts of USAG-1, 18S rRNA, GAPDH and beta-actin mRNA in the samples were estimated with standard curves representing the log of the input amount (the log starting with cDNA molecules) as the X axis and the threshold cycle as the Y axis. A relative standard curve (SC) for real-time PCR was used as a common set of samples that linked the experimental PCR plates together and permitted overall analysis of the

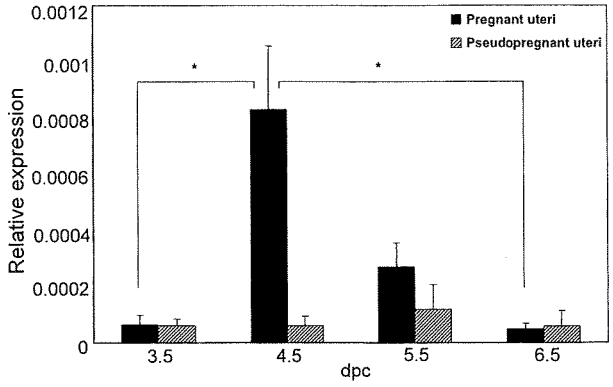

Fig. 2. Expression pattern of USAG-1 mRNA in the uteri of pregnant and pseudopregnant mice. Total RNA was extracted from the uteri of pregnant and pseudopregnant mice and subjected to real-time PCR analysis. The results are shown as the mean ± SE. Asterisks above the error bar indicate significant difference between the experimental groups. *: $P<0.05$.

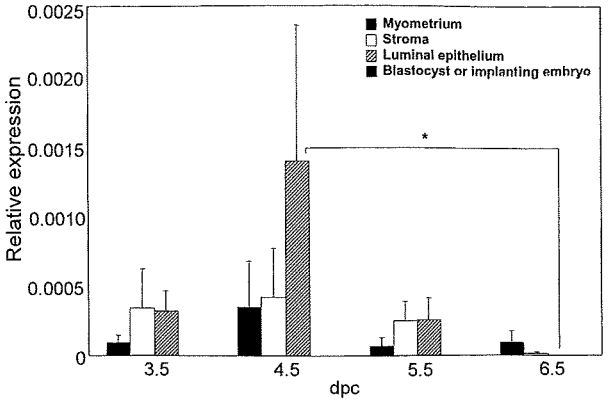

Fig. 3. Expression pattern of USAG-1 mRNA in the uterine tissues, blastocysts, and implanting embryos of pregnant mice. An LCM was used to separately collect uterine tissue samples from pregnant mice, and then total RNA was extracted from the tissue samples and subjected to real-time PCR analysis. The results are shown as the mean ± SE. Asterisks indicate significant differences between the experimental groups. *: $P<0.05$. The expression level of USAG-1 mRNA in the luminal epithelium at 4.5 dpc was significantly higher than that at 6.5 dpc ($P<0.05$).

samples. Preparation and utilization of this SC as a quality control of the efficiency of amplification of the PCR plate is described elsewhere [11]. The gene expression rate was obtained by normalizing the amount of USAG-1 with that of a housekeeping gene. Kidney mRNA was used as the standard.

Statistical analysis

All data are expressed as the mean ± standard error (SE). Statistical comparisons of the relative mRNA expressions of each gene between experimental groups were analyzed by two-way analysis of variance (ANOVA) followed by a *post hoc* test using StatView 4.5 (Abac Concepts, Berkeley, CA, USA). In all statistical tests, differences were considered significant when P was <0.05.

Results

Expression profiling of housekeeping genes in the pregnant uteri of the mice

The geNorm software (http://medgen.ugent.be/jvdesomp/genom) was used to select the most appropriate housekeeping gene as an internal control [12]. The internal control gene-stability measure (M) was calculated using geNorm. Since the M values of beta-actin, 18S rRNA, and GAPDH in the pregnant uteri were 4.134, 4.823 and 7.527, respectively, beta-actin was selected as the internal control gene for further experiments.

Expression pattern of USAG-1 mRNA in the uteri of the pregnant and pseudopregnant mice during the peri-implantation period

As shown in Fig. 2, USAG-1 mRNA expression in the uteri of the pregnant mice dramatically increased from 3.5 dpc to 4.5 dpc ($P<0.05$) and subsequently declined at 5.5 and 6.5 dpc ($P<0.05$). Although the differences were not statistically significant, the expression level of USAG-1 mRNA in the pregnant uterus was higher than that in the pseudopregnant uterus at 4.5 dpc. This difference may have been caused by the presence or absence of embryos in the reproductive tract.

Expression of USAG-1 mRNA in the myometrium, stroma, and luminal epithelium tissue of pregnant uteri during the peri-implantation period and in blastocysts and implanting embryos

The combination of LCM and real-time quantitative PCR revealed that the significant increase in USAG-1 mRNA seen in the pregnant

uterus at 4.5 dpc was localized mainly to the luminal epithelium (Fig. 3). On the other hand, the uterine stroma and myometrium exhibited minimal changes in USAG-1 mRNA expression at 3.5–5.5 dpc. As shown in Fig. 3, USAG-1 mRNA expression was undetectable in blastocysts collected from the uterus at 3.5 dpc and implanted embryos at 4.5, 5.5 and 6.5 dpc.

Discussion

USAG-1 expression in the reproductive tract was first found in the rat [4]. Induction of USAG-1 mRNA is restricted to the uterine glandular epithelial cells of the pregnant and pseudopregnant uteri on Day 5 [4]. Given the remarkably tight localization of its expression, USAG-1 might be involved in the onset of endometrial receptivity for implantation. It has been demonstrated that the expression of implantation-associated genes is influenced by ovarian hormones such as estrogen and progesterone [1]. We have previously examined the expression pattern of 16 implantation-associated genes, including USAG-1, during the estrous cycle in mice [8]. Expression of the majority of genes involved in the implantation process is temporally regulated during the estrous cycle [8]. However, interestingly, USAG-1 mRNA expression does not change during the estrous cycle in mice [8]. The results from these reports suggest that USAG-1 expression could be regulated by an embryonic signal(s) rather than an ovarian hormone(s).

The present study revealed that USAG-1 mRNA was expressed in both pregnant and pseudopregnant uteri throughout the peri-implantation period, i.e., from 3.5 dpc to 6.5 dpc, and was upregulated in pregnant animals on 4.5 dpc (Fig. 2). Furthermore, USAG-1 mRNA was localized exclusively in the luminal epithelium of the pregnant uteri at 4.5 dpc (Fig. 3). The expression of USAG-1 in blastocysts at 3.5 dpc and implanting embryos at 4.5 and 5.5 dpc was not detected by analysis using real-time quantitative PCR (Fig. 3). Furthermore, USAG-1 expression was not upregulated in pseudopregnant uteri during the peri-implantation period. These results indicate that the presence of embryos and/or a factor(s) from the embryos were an essential for upregulation of USAG-1 expression in the luminal epithelium at implantation in the mice. Stimuli from implanting embryos may influence uterine endometrial tissues and subsequently upregulate USAG-1 gene expression. We believe that blastocysts make their first molecular contact with the luminal epithelium for establishment of implantation and decidualization in conjunction with the expression of USAG-1. It is known that Mif is released from the luminal epithelium and superficial glandular epithelium by IFN-tau, which is produced by trophoblast cells in the cow [13], and that the epithelial cell-derived secreted adhesion proteins are regulated by progesterone and/or IFN-tau in sheep [14]. Although mice deficient in USAG-1 appear to be fertile [15] and the physiological function/s of USAG-1 for uterine receptivity and the process of implantation are still unclear, further studies using of gene targeting should clarify the role of USAG-1 in mammalian implantation.

Acknowledgements

This study was supported, in part, by Special Coordination Funds for Promoting Science and Technology from the Ministry of Education, Culture, Sports, Science and Technology of Japan. KM and DL contributed equally to this work. Pacific Edit reviewed the manuscript prior to submission.

References

1. **Ma WG, Song H, Das SK, Paria BC, Dey SK.** Estrogen is a critical determinant that specifies the duration of the window of uterine receptivity for implantation. *Proc Natl Acad Sci USA* 2003; 100: 2963–2968.
2. **Abrahamsohn PA, Zorn TM.** Implantation and decidualization in rodents. *J Exp Zool* 1993; 266: 603–628.
3. **Finn CA.** Menstruation: a nonadaptive consequence of uterine evolution. *Q Rev Biol* 1998; 73: 163–173.
4. **Simmons DG, Kennedy TG.** Uterine sensitization-associated gene-1: a novel gene induced within the

rat endometrium at the time of uterine receptivity/sensitization for the decidual cell reaction. *Biol Reprod* 2002; 67: 1638–1645.

5. **Laurikkala J, Kassai Y, Pakkasjarvi L, Thesleff I, Itoh N.** Identification of a secreted BMP antagonist, ectodin, integrating BMP, FGF, and SHH signals from the tooth enamel knot. *Dev Biol* 2003; 264: 91–105.
6. **Yanagita M, Oka M, Watabe T, Iguchi H, Niida A, Takahashi S, Akiyama T, Miyazono K, Yanagisawa M, Sakurai T.** USAG-1: a bone morphogenetic protein antagonist abundantly expressed in the kidney. *Biochem Biophys Res Commun* 2004; 316: 490–500.
7. **Altschul SF, Madden TL, Schaffer AA, Zhang J, Zhang Z, Miller W, Lipman DJ.** Gapped BLAST and PSI-BLAST: a new generation of protein database search programs. *Nucleic Acids Res* 1997; 25: 3389–3402.
8. **Lee DS, Yanagimoto Ueta Y, Xuan X, Igarashi I, Fujisaki K, Sugimoto C, Toyoda Y, Suzuki H.** Expression patterns of the implantation-associated genes in the uterus during the estrous cycle in mice. *J Reprod Dev* 2005; 51: 787–798.
9. **Burbach GJ, Dehn D, Del Turco D, Deller T.** Quantification of layer-specific gene expression in the hippocampus: effective use of laser microdissection in combination with quantitative RT-PCR. *J Neurosci Methods* 2003; 131: 83–91.
10. **Uchide T, Masuda H, Mitsui Y, Saida K.** Gene expression of vasoactive intestinal contractor/endothelin-2 in ovary, uterus and embryo: comprehensive gene expression profiles of the endothelin ligand-receptor system revealed by semi-quantitative reverse transcription-polymerase chain reaction analysis in adult mouse tissues and during late embryonic development. *J Mol Endocrinol* 1999; 22: 161–171.
11. **Wilhelm J, Pingoud A, Hahn M.** Validation of an algorithm for automatic quantification of nucleic acid copy numbers by real-time polymerase chain reaction. *Anal Biochem* 2003; 317: 218–225.
12. **Vandesompele J, De Preter K, Pattyn F, Poppe B, Van Roy N, De Paepe A, Speleman F.** Accurate normalization of real-time quantitative RT-PCR data by geometric averaging of multiple internal control genes. *Genome Biol* 2002; 3: RESEARCH0034.
13. **Wang B, Goff AK.** Interferon-tau stimulates secretion of macrophage migration inhibitory factor from bovine endometrial epithelial cells. *Biol Reprod* 2003; 69: 1690–1696.
14. **Spencer TE, Bazer FW.** Conceptus signals for establishment and maintenance of pregnancy. *Reprod Biol Endocrinol* 2004; 2: 49.
15. **Yanagita M, Okuda T, Endo S, Tanaka M, Takahashi K, Sugiyama F, Kunita S, Takahashi S, Fukatsu A, Yanagisawa M, Kita T, Sakurai T.** Uterine sensitization-associated gene-1 (USAG-1), a novel BMP antagonist expressed in the kidney, accelerates tubular injury. *J Clin Invest* 2006; 116: 70–79.

REPRODUCTION
RESEARCH

Effect of pressure at primary drying of freeze-drying mouse sperm reproduction ability and preservation potential

Yosuke Kawase, Toshio Hani, Nobuo Kamada, Kou-ichi Jishage and Hiroshi Suzuki[1,2]

Chugai Research Institute for Medical Science, Inc., Shizuoka, Japan, [1]Research Unit for Functional Genomics, National Research Center for Protozoan Diseases, Obihiro University of Agriculture and Veterinary Medicine, Obihiro, Hokkaido, Japan and [2]Department of Developmental and Medical Technology, Graduate School of Medicine, The University of Tokyo, Tokyo, Japan

Correspondence should be addressed to H Suzuki; Email: hisuzuki@obihiro.ac.jp

Abstract

Freeze-dried spermatozoa are capable of participating in normal embryonic development after injection into oocytes and thus useful for the maintenance of genetic materials. We recently reported that long-term preservation of freeze-dried mouse spermatozoa by conventional methods requires temperatures lower than −80 °C. Successful permanent preservation of mouse spermatozoa at much higher temperatures requires thorough investigation of the freeze-drying procedure. Thus, we examined the relationship between the pressure at primary drying and the preservation potential of freeze-dried mouse spermatozoa. Three different primary drying pressures were applied to evaluate the effect of pressure on freeze-dried spermatozoa under varying storage conditions and the rate of development measured. The developmental rate of embryos to the blastocyst stage from intracytoplasmic sperm injection by freeze-dried spermatozoa at pressures of 0.04, 0.37, and 1.03 mbar without storage were 59% (337/576), 71% (132/187), and 33% (99/302) respectively. When stored at 4 °C for 6 months, the rate was 13% (48/367), 50% (73/145), and 36% (66/182) respectively. These results show that primary drying pressure is an influential factor in the long-term preservation of freeze-dried mouse spermatozoa.

Reproduction (2007) **133** 841–846

Introduction

In the last decade, numerous reports have shown that freeze-dried mouse spermatozoa are capable of participating in normal embryonic development after injection into oocytes (Wakayama & Yanagimachi 1998, Kusakabe *et al.* 2001, Kaneko *et al.* 2003*a*,*b*, Ward *et al.* 2003, Kawase *et al.* 2005). Freeze-dried mouse spermatozoa are most efficiently stored for extended periods, several to tens of decades, at temperatures lower than −80 °C (Kawase *et al.* 2005). However, maintaining such low temperatures over a long period of time puts the samples at risk of loss from technical difficulties (e.g. power failure) and requires a relatively high initial investment. Although freeze-dried spermatozoa can be stored for 1.5 years (Ward *et al.* 2003), this length of time is insufficient for either the maintenance of genetically modified mouse strains or mutant mice in saturation mutagenesis projects. Long-term preservation at ambient temperatures would be ideal. The freeze-drying process is of importance, especially the primary drying process; however, no study of pressure at primary drying of spermatozoa has been reported. Here, we focused on the pressure at primary drying and found 0.37 mbar to be the optimum pressure for preservation of freeze-dried mouse spermatozoa at much higher temperatures.

Materials and Methods

Animals

F1 (B6C3F1) mice were purchased from Clea Japan (Tokyo, Japan). All the mice were housed in polycarbonate cages and maintained under a specific pathogen-free environment in light-controlled lights on from 0500 to 1900 h and air-conditioned rooms (temperature, 24±1 °C; humidity, 50±10%). The mice had free access to standard laboratory chow (CE-2, Clea Japan). The Institutional Animal Care and Use Committee of Chugai Pharmaceutical reviewed the protocols and confirmed that the animals used in this study were cared for and used under the Guiding Principles for the Care and Use of Research Animals promulgated by Chugai Pharmaceutical.

ISSN 1470–1626 (paper) 1741–7899 (online)

DOI: 10.1530/REP-06-0170
Online version via www.reproduction-online.org

Freeze-drying and preservation of spermatozoa

The procedure for freeze-drying was essentially the same as that described by Kaneko *et al.* (2003*a*) and Kawase *et al.* (2005). The six epididymides from three B6C3F1 male mice were removed and a dense sperm mass was squeezed out of each cauda epididymis from a cut made with scissors. The total sperm mass was gently placed in 9 ml EGTA Tris–HCl-buffered solution (50 mM EGTA, 50 mM NaCl, and 10 mM Tris–HCl, pH 8.0; Kaneko *et al.* 2003*a*) in a tube (352059, Becton Dickinson Labware, NJ, USA) and kept at 37 °C for 10 min. The sperm suspension at a concentration of $15–38\times10^6$ cells/ml was divided into 18 aliquots. Each aliquot of 500 μl was put into an amber vacuum vial for freeze-drying (V-2B, Nichiden-rika Glass Co. Ltd., Kobe, Japan). The vials were plunged into liquid nitrogen (~ −196 °C) for 5 min and then transferred to a programmable freeze-dryer (BETA2-16, Martin Christ Gefriertrocknungsanlagen GmbH, Osterode am Harz, Germany), which had been pre-cooled to −30 °C. The freeze-drying conditions consisted of primary drying at a pressure of 0.04 mbar for 8 h, 0.37 mbar for 13 h, or 1.03 mbar for 13 h and secondary drying at a pressure of 0.001 mbar for 6 h. More time is required for complete drying when lower pressures are provided at primary drying. The inside pressure of the vials at the time of sealing was 0.001 mbar and pressure reduction was within 5 min. The vials were stored at 4 or 30 °C until use. Immediately before ICSI, the vials of freeze-dried spermatozoa were unsealed, and the spermatozoa were hydrated by adding 500 μl sterile distilled water. To maintain a similar composition of sperm suspension before and after freeze-drying, distilled water was added rather than a medium such as Hepes-buffered culture medium.

Comet assay for DNA damage

DNA damage of the spermatozoa from freeze-drying and subsequent preservation was assessed by single-cell gel electrophoresis (comet assay; Hughes *et al.* 1997, Steel *et al.* 1999, Cho *et al.* 2003). Evaluation of the shape of the DNA 'comet' tail and migration pattern gives an assessment of DNA damage. The sperm suspension was suspended in Comet LMAgarose (1% low-temperature melting agarose, Trevigen, Gaithersburg, MD, USA) at a ratio 1:10 (v/v). With the addition of molten LMAgarose at 37 °C, 25 μl sperm suspension was immediately placed on a CometSlide (Trevigen). The slides were placed flat in a refrigerator at 4 °C for 10 min and then submerged in 23 ml lysis solution (Trevigen) at 4 °C for 60 min. Next, 2.5 ml 10 mM dithiothreitol was added and the slides were then incubated for 30 min at 4 °C, followed by the addition of 2.5 ml of 4 mM LIS (lithium diiodosalicylate) and incubation for 90 min at room temperature. The slides were then kept in an alkaline solution (>pH 13) for 20 min at room temperature in the darkness. The slides were subjected to electrophoresis in 1×TBE (Tris-borate EDTA) buffer at 25 V for 10 min, stained with SYBR Green (Trevigen), and analyzed under a microscope (IX-70, Olympus Co., Tokyo, Japan). DNA damage of freeze-dried spermatozoa was assessed by Comet assay twice per experimental group. Comet tail length is the distance the damaged DNA has migrated from the sperm head and gives an estimate of the extent of the damage.

Preparation of oocytes

Mature B6C3F1 females were induced to superovulate by i.p. injections of 5 IU equine chorionic gonadotropin (Serotrophin, Teikokuzoki Co., Tokyo, Japan) and 5 IU human chorionic gonadotropin (hCG; Puberogen, Sankyo Co., Tokyo, Japan) 48 h later. Freshly ovulated oocytes were collected from oviducts 15–16 h after being injected with hCG. The oocytes were treated with 0.1% hyaluronidase (280 units/mg; H-3506, SIGMA Chemical Co.) in Whitten's medium (Whitten 1971) supplemented with 100 μM ethylene diamine tetraacetic acid disodium salt (EDTA; Abramczuk *et al.* 1977) to remove cumulus cells.

Intracytoplasmic sperm injection

After rehydration of the freeze-dried spermatozoa as described above, one part of the sperm suspension was thoroughly mixed with nine parts 0.9% NaCl solution (saline) containing 12% (w/v) polyvinyl pyrrolidone (PVP, No. 99219, Mt. 360 000, Irvine Scientific, Santa Ana, CA, USA). Two drops (~5 μl each) of 12% PVP saline and two drops of 20 mM Hepes-buffered Whitten's medium containing 0.1% polyvinyl alcohol (PVA, P-8136, MW 30 000–70 000, Sigma) were linearly placed on the injection chamber (Kawase *et al.* 2001) and then covered with mineral oil (M-8410, embryo tested, Sigma). The first drop of 12% PVP saline was used to wash the injection pipette, and added to the second drop was 1–2 μl of the diluted sperm suspension. The first drop of the medium was used to remove spermatozoa that had attached to the surface of the injection pipette. The cumulus-free oocytes were placed in the second drop of Hepes-buffered Whitten's medium. The injection chamber with the spermatozoa and oocytes was transferred onto the stage of an inverted microscope maintained at ~18 °C (MATS-555RSP, Tokai Hit, Shizuoka, Japan).

The procedure for micromanipulation of the sperm for ICSI was essentially the same as that described previously (Kimura & Yanagimachi 1995, Kawase *et al.* 2001). The sperm head was separated from the tail by applying three or four piezo pulses (controller setting: speed 2, intensity 2) to the head–tail junction of the spermatozoon. In the same manner, a total of 3–5

Table 1 Effect of vacuum pressure at primary drying on the *in vitro* development of embryos generated by ICSI of freeze-dried, non-stored spermatozoa.

Vacuum pressure (mbar)	No. of oocytes injected	No. (%) of oocytes survived	No. (%) of oocytes fertilized[a]	No. (%) of embryos developed to two-cell[b]	No. (%) of embryos developed to blastocyst[b]
0.04	864	608 (70)[a]	576 (95)[a]	557 (97)[a]	337 (59)[a]
0.37	253	194 (77)[ab]	187 (96)[a]	181 (97)[a]	132 (71)[b]
1.03	404	317 (78)[b]	302 (95)[a]	288 (95)[a]	99 (33)[c]

Different superscript letters within a column indicate significantly different values ($P<0.05$).
[a]Percentage of oocytes survived. [b]Percentage of oocytes fertilized.

isolated sperm heads were lined up in the pipette. Several piezo pulses (controller setting: speed 2, intensity 2) were applied to advance the tip of the injection pipette to the surface of zona pellucida; the pipette was advanced mechanically while applying slightly negative pressure. The oolemma was punctured using 1–2 piezo pulses (controller setting: speed 1, intensity 1). A single sperm head was then expelled into the ooplasm accompanied with a minimum amount of medium. Following retrieval of as much as possible of the medium, the injection pipette was withdrawn while applying negative pressure to the pipette.

Culture of oocytes and embryos transfer

Sperm-injected oocytes were incubated and cultured in Whitten's medium supplemented with 100 μM EDTA at 37.5 °C in 5% CO_2 and 95% air. After 6-h ICSI, live oocytes showing two distinct pronuclei and a second polar body were considered fertilized. The fertilized eggs were further cultured in Whitten's medium supplemented with 100 μM EDTA for 96 h at 37.5 °C in 5% CO_2 95% air. About 96 h after ICSI, the blastocysts were transferred into the uteri of pseudopregnant ICR recipients (CLEA Japan) 2.5 days *postcoitum* (dpc) using the embryo transfer method described by Suzuki *et al.* (1994). The recipient females were killed on 18.5 dpc to determine the number of implantation sites by macroscopic check and the number of term fetuses.

Statistical analysis

Data presented in this study were analyzed statistically by the χ^2-test and Tukey's test for non-parametric multiple comparisons (SAS version 6.12, SAS Institute, Cary, NC, USA). In all statistical tests, the difference was considered significant when $P<0.05$.

Results

The developmental rates to the blastocyst stage of embryos from ICSI by freeze-dried spermatozoa without storage, with storage at 30 °C for 3 days, and at 4 °C for 6 months are shown in Tables 1–3. All the three storage conditions showed the highest rate of embryonic development when primary drying was performed at 0.37 mbar. In addition, the number of live-term fetuses produced was higher at 0.37 mbar than at other pressures for groups non-stored and stored at 4 °C for 6 months although the difference was not significant (Table 4). All fetuses were morphological normal – some of the mice have since been mated and delivered normal offspring. A numerical indicator for overall efficiency of mouse production after ICSI using freeze-dried mouse spermatozoa was determined by dividing the ratio of the number of embryos that developed blastocysts to the number of fertilized oocytes, by the ratio of the number of live-term fetuses to the number of blastocysts transferred (Fig. 1). With storage at 4 °C for 6 months, the overall efficiency from a pressure of 0.37 mbar (10.3) or 1.03 mbar (8.8) was significantly higher than 0.04 mbar (1.1). Moreover, with a pressure of 0.37 mbar (25.7) non-stored, the overall efficiency after ICSI was significantly higher than for 0.04 mbar (17.5) or 1.03 mbar (6.62). The results showed that blastocyst formation was significantly higher when primary drying was performed at 0.37 mbar than at 0.04 and 1.03 mbar irrespective of the storage conditions (non-stored, 30 °C for 3 days, or 4 °C for 6 months; Tables 1–3, Fig.1).

Percentages of spermatozoa with comet tails freeze-dried at 4 °C for 6 months were 100 and 96%, and stored at 30 °C for 3 days were 4 and 100% respectively. Although there was no significant difference between the percentages of spermatozoa with damaged DNA at 0.04 mbar stored at 30 °C for 3 days and of those without

Table 2 Effect of vacuum pressure at primary drying on the *in vitro* development of embryos generated by ICSI of freeze-dried spermatozoa stored at 30 °C for 3 days.

Vacuum pressure (mbar)	No. of oocytes injected	No. (%) of oocytes survived	No. (%) of oocytes fertilized[a]	No. (%) of embryos developed to two-cell[b]	No. (%) of embryos developed to blastocyst[b]
0.04[c]	251	175 (70)[a]	170 (97)[a]	162 (95)[a]	34 (20)[a]
0.37	161	117 (73)[a]	113 (97)[ab]	111 (98)[a]	61 (54)[b]
1.03	187	145 (78)[a]	132 (91)[b]	129 (98)[a]	25 (19)[a]

Different superscript letters within a column indicate significantly different values ($P<0.05$).
[a]Percentage of oocytes survived. [b]Percentage of oocytes fertilized. [c]Data from Kawase *et al.* (2005).

Table 3 Effect of vacuum pressure at primary drying on the *in vitro* development of embryos generated by ICSI of freeze-dried spermatozoa stored at 4 °C for 6 months.

Vacuum pressure (mbar)	No. of oocytes injected	No.(%) of oocytes survived	No. (%) of oocytes fertilized[a]	No. (%) of embryos developed to two-cell[b]	No. (%) of embryos developed to blastocyst[b]
0.04[c]	522	404 (77)[a]	367 (91)[a]	346 (94)[a]	48 (13)[a]
0.37	213	156 (73)[a]	145 (93)[ab]	142 (98)[a]	73 (50)[b]
1.03	267	187 (70)[a]	182 (97)[b]	179 (98)[a]	66 (36)[c]

Different superscript letters within a column indicate significantly different values ($P<0.05$).
[a]Percentage of oocytes survived. [b]Percentage of oocytes fertilized. [c]Data from Kawase *et al.* 2005.

Table 4 Effect of vacuum pressure at drying on the *in vivo* development of embryos generated by ICSI using freeze-dried spermatozoa.

Vacuum pressure (mbar)	Storage temperature (°C)	Sperm storage time (months)	No. of blastocysts transferred	No. (%) of implantation sites	No. (%) of live-term fetuses
0.04	RT	non-stored	194	137 (71)[a]	58 (30)[a]
0.37	RT	non-stored	132	93 (70)[a]	48 (36)[a]
1.03	RT	non-stored	99	70 (71)[a]	20 (20)[a]
0.04	4	6	48	28 (58)[a]	4 (8)[a]
0.37	4	6	73	39 (53)[a]	15 (21)[a]
1.03	4	6	66	56 (85)[b]	16 (24)[a]

Values within a column with the same superscript are not significantly different ($P>0.05$).

storage, developmental rates to the blastocyst stage after ICSI was significantly reduced with storage. In contrast, spermatozoa freeze-dried at 0.37 mbar and then assessed immediately (non-stored) or after storage at 4 °C for 6 months did not have comet tails (Fig. 2, Table 5). At the primary drying pressure of 0.04 mbar, the average comet tail length of spermatozoa stored at 30 °C for 3 days and at 4 °C stored for 6 months was 0.7 ± 3.4 and 20.2 ± 5.0 μm ($P<0.05$), and at 1.03 mbar, average tail length was 23.4 ± 6.2 and 23.0 ± 8.4 μm ($P>0.05$) respectively (Table 5).

Discussion

Preservation of freeze-dried spermatozoa for extended periods of time, potential 100 years or more, by current methods would require storage temperatures lower than −80 °C (Kawase *et al.* 2005). Successful long-term preservation of mouse spermatozoa at higher temperatures requires investigation and modification of the current freeze-drying method. Although the primary drying phase is one of the most important processes in the freeze-drying process of spermatozoa, there have been no studies on the primary drying pressure. Nail *et al.* (2002) reported that the pressure in the freeze-dryer has to be lower than the vapor pressure of ice at the temperature of the product, and pressures of 0.04, 0.37, and 1.03 mbar are appropriate for materials stored at −50, −30, and −20 °C respectively. Thus, in this study, we selected primary drying pressures of 0.37 and 1.03 mbar, in addition to the commonly used 0.04 mbar. Primary drying is characterized by the specimen undergoing rapid shrinkage as the ice sublimates (ice forming water vapor and leaving the specimen). In this study, ~98% of the total volume of water (0.51 g wet weight) was lost. During this step, evaporative cooling keeps the temperatures low. When most ice has sublimed, heat is no longer lost by evaporative cooling and the temperature of the product usually increases sharply toward shelf temperature. Since the driving force for freeze-drying is the vapor pressure of the ice, from the standpoint of process efficiency, it is important to keep the product temperature as high as possible during primary drying (Nail *et al.* 2002). As we reported recently, freeze-dried sperm kept at a pressure of 0.04 mbar and then stored at 30 °C for 3 days or at 4 °C for 3 months had the same rate of blastocyst formation (Kawase *et al.* 2005). Although a pressure of 0.37 mbar gave the best results when

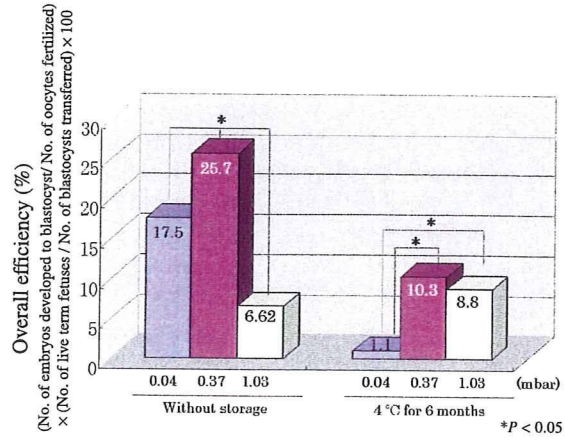

Figure 1 Overall efficiency of mouse production from ICSI using freeze-dried spermatozoa. Sperm were dried at 0.04 mbar (blue bar), 0.37 mbar (purple bar), or 1.03 mbar (yellow bar) and then used for ICSI non-stored (left) or after storage at 4 °C for 6 months (right).